

^3He adsorbed on molecular hydrogen surfaces

M. C. Gordillo^{1,2*}

¹*Departamento de Sistemas Físicos, Químicos y Naturales,
Universidad Pablo de Olavide, Carretera de Utrera km 1, E-41013 Sevilla, Spain and*

²*Instituto Carlos I de Física Teórica y Computacional,
Universidad de Granada, E-18071 Granada, Spain*

J. Boronat³

³*Departament de Física, Universitat Politècnica de Catalunya, Campus Nord B4-B5, 08034 Barcelona, Spain*

(Dated: July 18, 2024)

Using a diffusion Monte Carlo (DMC) technique, we calculated the phase diagram of ^3He adsorbed on a first solid layer of a molecular hydrogen isotope (H_2 , HD and D_2) on top of graphite. The results are qualitatively similar in all cases: a two-dimensional gas spanning from the infinite dilution limit to a second-layer helium density of $0.048 \pm 0.004 \text{ \AA}^{-2}$. That gas is in equilibrium with a $7/12$ commensurate structure, more stable than any incommensurate triangular solid of similar density. These findings are in reasonably good agreement with available experimental data.

I. INTRODUCTION

At the heart of any Monte Carlo calculation lies the same principle that allow us to compute a simple integral by a hit-and-miss method, modified by the introduction of techniques to reduce the statistical variance. The first relevant application of that proposal was the calculation of the properties of a gas of hard spheres in the seminal paper by Metropolis *et al* [1]. Thus, the basic idea behind the Monte Carlo method consists in transforming the expression that describe the phenomena we are interested in into an integral, and apply a modification of that simple integration recipe to calculate the desired magnitude [2]. For classical averages this is straightforward, since the equations that define them are already integrals defined in a multidimensional space. The application to quantum systems is more involved but it is now currently used in a set of methods known globally as quantum Monte Carlo (QMC).

The simplest QMC method consists in the application of the variational principle of Quantum Mechanics to calculate the energy and other observables for a proposed many-body wavefunction [3]. The accuracy of this method, known as variational Monte Carlo (VMC), depends on the quality of that wavefunction. This constraint can be removed by using the diffusion Monte Carlo (DMC) algorithm [4], which tackles directly the imaginary-time Schrödinger equation by using the connection between a random walk and the diffusion equation. Therefore, DMC is able, at least in principle, to produce the real ground state of any many-body system by improving upon that initial guess. That technique has been applied successfully to many bosonic and fermionic ensembles of particles [3, 5]. In this work, we are going to use the DMC algorithm to study the properties of a system that includes either fermions (^3He atoms, HD

molecules) or a mixture of bosons and fermions (^3He adsorbed on top of a H_2 or a D_2 layer).

The calculations presented in this work are prompted by experimental results on ^3He adsorbed on a double HD layer on top of graphite, both using NMR techniques [6–9] or calorimetric measurements [6, 10–13]. Those findings are part of a long series of studies on ^3He on clean and preplated graphite, both from the experimental [14–23] and theoretical [24, 25] points of view. All those experimental studies of ^3He on HD preplated graphite agree in finding both a liquid/gas and a low-density commensurate solid. In this work, we will address the nature of both phases by means of DMC calculations.

The rest of the paper is organized as follows. In the next section, we describe the DMC algorithm and its application to obtain the equation of state of ^3He on a single molecular hydrogen layer on top of graphite. In Sec. III, we report the results obtained for the equations of state of the ^3He films adsorbed on different molecular hydrogen isotopes. Finally, Sec. IV comprises a brief summary and a discussion of the main conclusions.

II. METHOD

The most ambitious approach to the quantum many-body problem, from a microscopic point of view, is to solve its corresponding Schrödinger equation. The diffusion Monte Carlo (DMC) method does so stochastically, starting by its imaginary-time counterpart [5]:

$$-\frac{\partial\Psi(\mathbf{R}, t)}{\partial t} = (H - E)\Psi(\mathbf{R}, t), \quad (1)$$

with \mathbf{R} standing for the positions of all the atoms/molecules in the system. The Hamiltonian H of the system, composed by ^3He atoms and hydrogen

* Corresponding author: cgorbar@upo.es

molecules, is given by

$$H = \sum_{\alpha} \sum_{i=1}^{N_{\alpha}} \left[-\frac{\hbar^2}{2m_{\alpha}} \nabla_i^2 + V_{\text{ext}}^{(\alpha)}(x_i, y_i, z_i) \right] + \quad (2)$$

$$\sum_{\alpha} \sum_{i < j}^{N_{\alpha}} V_{\text{pair}}^{(\alpha, \alpha)}(r_{ij}) + \sum_{\alpha} \sum_{\beta} \sum_{i}^{N_{\alpha}} \sum_{j}^{N_{\beta}} V_{\text{pair}}^{(\alpha, \beta)}(r_{ij}).$$

As in previous literature, we considered graphite as a rigid structure, i.e., its influence on the behavior of ^3He and hydrogen molecules will be modeled by an external potential, $V_{\text{ext}}^{(\alpha)}(x_i, y_i, z_i)$, different for each species $\alpha = [^3\text{He}, (\text{H}_2, \text{HD}, \text{D}_2)]$. To release that constraint by allowing the carbon atoms to move around their crystallographic positions does not change the behavior of the first layer of molecular hydrogen at the densities considered in this work [26]. In Eq. 2, the coordinates x_i , y_i , and z_i correspond to each of the N_{α} or N_{β} (Helium *or* Hydrogen) adsorbate particles with mass m_{α} . All the individual adsorbate-carbon interactions were explicitly considered, in a full rendition of graphite as a corrugated structure made up of parallel layers separated 3.35 Å in the z direction. In all cases, those $V_{\text{ext}}^{(\alpha)}(x_i, y_i, z_i)$ potentials were taken to be of the Lennard-Jones type and no distinction was made between different hydrogen isotopes [27]. In particular, the He-C interaction was taken from Ref. 28, while the $(\text{H}_2, \text{HD}, \text{D}_2)$ -C potential was the one derived in Ref. 29.

In the Hamiltonian (2), we have as many expressions for $V_{\text{pair}}^{(\alpha, \beta)}$ as possible adsorbate pairs, i.e., He-He, He- $(\text{H}_2, \text{HD}, \text{D}_2)$ and $(\text{H}_2, \text{HD}, \text{D}_2)$ - $(\text{H}_2, \text{HD}, \text{D}_2)$. For the ^3He - ^3He interaction, we used the standard Aziz potential [30], while for any hydrogen-hydrogen interaction we resort to the Silvera and Goldman expression [27, 31]. The Helium- H_2 potential was taken from Ref. [32], previously used in the study of small clusters including ^4He - H_2 mixtures [33]. What all those potentials have in common is that they are isotropic interactions, depending only on the distance r_{ij} between particles i and j . In the case of molecular hydrogen, an ellipsoid, the Silvera and Goldman potential was built to reproduce the isotropic properties of solid phases and does so very successfully. In all cases, the hydrogen molecules were not kept fixed but allowed to move around their crystallographic positions.

The solution of Eq. (1) can be formally written as

$$\Psi(\mathbf{R}', t + \Delta t) = \int G(\mathbf{R}', \mathbf{R}, \Delta t) \Psi(\mathbf{R}, t) d\mathbf{R}, \quad (3)$$

with t the imaginary time. The Green's function is given by

$$G(\mathbf{R}', \mathbf{R}, \Delta t) = \langle \mathbf{R}' | \exp[-(H - E)\Delta t] | \mathbf{R} \rangle, \quad (4)$$

with E an energy close to the ground-state value. By remembering that $\Psi(\mathbf{R}, t)$ can be expanded in terms of a complete set of the Hamiltonian's eigenfunctions, $\Phi_i(\mathbf{R})$,

with eigenvalues E_i , as

$$\Psi(\mathbf{R}, t) = \sum_i c_i e^{-(E_i - E)t} \Phi_i(\mathbf{R}), \quad (5)$$

we can see that, successive applications of Eq. 3 on any initial approximation to the exact wavefunction, will project to the ground state in the $t \rightarrow \infty$ limit, i.e, this method produces a zero-temperature estimation. However, given the very low temperatures at which the relevant experiments are performed, usually of the order of the mK, that solution is expected to be a very good approximation to what is observed. Any iterative application of Eq. 3 constitutes a Monte Carlo step in the DMC algorithm.

Unfortunately, this procedure, even though it is formally correct, produces very noisy estimations [3]. To reduce the statistical variance of the results to a manageable level, one introduces importance sampling. This is done by means of a time-independent trial wave function, $\psi(\mathbf{R})$, as close as possible to the exact solution of Eq. 1. We define then an auxiliary function, $f(\mathbf{R}, t)$, as

$$f(\mathbf{R}, t) = \psi(\mathbf{R}) \Psi(\mathbf{R}, t), \quad (6)$$

that introduced in Eq. 1 gives

$$-\frac{\partial f(\mathbf{R}, t)}{\partial t} = A(\mathbf{R}, t) f(\mathbf{R}, t), \quad (7)$$

with

$$A(\mathbf{R}, t) = -\frac{\hbar^2}{2m_i} \nabla_i^2 + \frac{\hbar^2}{2m_i} F(\mathbf{R}) + [E_L(\mathbf{R}) - E]. \quad (8)$$

At difference with Eq. (1), Eq. 7 includes a drift term, with $F(\mathbf{R}) = 2\psi(\mathbf{R})^{-1} \nabla \psi(\mathbf{R})$, that guides the stochastic process to the regions where the trial function is larger. $E_L(\mathbf{R}) = \psi(\mathbf{R})^{-1} H \psi(\mathbf{R})$ is the so-called local energy, whose mean value is the exact energy of the system.

We considered ^3He adsorbed on a single molecular hydrogen layer, contrarily to the experimental setups of Refs. 6–13, in which Helium is adsorbed on top of two or more [9] HD sheets. To include two layers would have doubled the number of hydrogen molecules in our simulations (see below), and would have implied a considerable increase in the computational complexity and in the simulation time. Moreover, the vertical distance between the ^3He sheet and a second hydrogen layer closest to the graphite would have been large enough (around 6 Å, see for instance the distribution of H_2 layers in Ref. 34) to make the influence of that layer on the Helium equation of state negligible, apart from a nearly constant correction in the value of the binding energy. That correction is expected to be small given the shallowness of the He- $(\text{H}_2, \text{HD}, \text{D}_2)$ potential [32]. In any case, ours is a new quasi-2D ^3He system whose behaviour could be directly compared with an experimental setup with a single hydrogen layer on top of graphite.

Taking all that in mind, and following previous work on ^3He films [24, 25], we considered a two-layer trial wave function of the form

$$\psi(\mathbf{r}_1, \mathbf{r}_2, \dots, \mathbf{r}_N) = \psi_1(\mathbf{r}_1, \mathbf{r}_2, \dots, \mathbf{r}_{N_1}) \times \psi_2(\mathbf{r}_{N_1+1}, \mathbf{r}_N, \dots, \mathbf{r}_N), \quad (9)$$

with N_1 the number of hydrogen molecules in the single layer adsorbed on the graphite surface and N the total number of particles ($\text{H}_2/\text{HD}/\text{D}_2$ molecules and ^3He atoms). The number of ^3He atoms in the second layer is thus $N_2 = N - N_1$. The trial wave function for the upper ^3He layer is [24]

$$\psi_2(\mathbf{r}_{N_1+1}, \mathbf{r}_{N_1+2}, \dots, \mathbf{r}_N) = D^\uparrow D^\downarrow \prod_{i=N_1+1}^N u_3(\mathbf{r}_i) \times \prod_{i<j}^{N_2} \exp\left[-\frac{1}{2}\left(\frac{b_3}{r_{ij}}\right)^5\right], \quad (10)$$

where D^\uparrow and D^\downarrow are Slater determinants including two-dimensional plane waves depending on the second layer particle coordinates (with spins up and down) and whose periodicity is determined by the size of the simulation cell. In all cases, we considered the same number of spin-up and spin-down ^3He atoms. The coordinates in the Slater determinants were corrected by backflow terms in the standard way [35, 36],

$$\tilde{x}_i = x_i + \lambda \sum_{j \neq i} \exp[-(r_{ij} - r_b)^2 / \omega^2] (x_i - x_j) \quad (11)$$

$$\tilde{y}_i = y_i + \lambda \sum_{j \neq i} \exp[-(r_{ij} - r_b)^2 / \omega^2] (y_i - y_j). \quad (12)$$

The optimal values for the parameters in the backflow term were those of the bulk three-dimensional system [37, 38], i.e., $\lambda = 0.35$; $\omega = 1.38 \text{ \AA}$, and $r_b = 1.89 \text{ \AA}$.

The one-body function $u_3(\mathbf{r})$ is the numerical solution of the Schrödinger equation that describes a single ^3He atom on top of a hydrogen first layer of density 0.095 \AA^{-2} . This is the largest experimental HD density before a promotion to a second HD layer on top of graphite happens [39]. This density is the same as for H_2 promotion to the a second layer [34, 40, 41], and comparable to the density D_2 needs to jump to that second layer [40], 0.100 \AA^{-2} . That density is also of the same order of magnitude as the corresponding to the uppermost HD layer in a $^3\text{He}/\text{HD}/\text{HD}$, studied experimentally in Refs. 6–13 ($\sim 0.092 \text{ \AA}^{-2}$), whose results are directly comparable to those of the present work. With all those considerations in mind, and to avoid as much as possible size effects, we considered a 14×8 first layer cell of molecules separated 3.48 \AA from each other, i.e., a $48.72 \times 48.22 \text{ \AA}^2$ simulation cell comprising 224 hydrogen molecules. The remaining parameter b_3 is 2.96 \AA , as in previous literature [24] and defines the Jastrow part of the trial wavefunction, designed to avoid the unphysical situation in which two Helium atoms are located one on top of each other.

The part of the trial wave function corresponding to the layer in contact with the graphite surface, that contains the different hydrogen isotopes is taken as

$$\psi_1(\mathbf{r}_1, \dots, \mathbf{r}_{N_1}) = \prod_i^{N_1} u(\mathbf{r}_i) \prod_{i<j}^{N_1} \exp\left[-\frac{1}{2}\left(\frac{b}{r_{ij}}\right)^5\right] \times \prod_i^{N_1} \exp\{-a_1[(x_i - x_{\text{site}})^2 + (y_i - y_{\text{site}})^2]\}. \quad (13)$$

As before, the function $u(\mathbf{r})$ is the numerical solution to the Schrödinger equation that defines the interaction between a single hydrogen molecule and the graphite surface, and it depends on the mass of the different species (H_2, HD or D_2) on top of the carbon layer. The variational Jastrow parameter b was fixed to 3.195 \AA for all isotopes, since in previous literature dealing with similar systems [34, 40, 42, 43] it was found to be independent of the mass.

The last term in Eq. 13 pines the atoms around their crystallographic positions $(x_{\text{site}}, y_{\text{site}})$, in this case the ones defining a triangular lattice of density 0.095 \AA^{-2} . The a_1 's parameters entering that function depend on the mass of the hydrogen adsorbate and to obtain them we performed several VMC calculations using Eq. 13 as a wavefunction for different values of a_1 . The parameters that produced the lowest energies for the different molecular isotopes were $a_1 = 1.19 \text{ \AA}^{-2}$ (H_2), 1.61 \AA^{-2} (HD) and 2.02 \AA^{-2} (D_2).

Eq. 10 would define adequately a gas or a liquid ^3He layer. On the other hand, to model efficiently a second-layer ^3He solid, one fixes those atoms to the crystallographic positions corresponding to the structure we are interested in. To do so, we will have to multiply Eq. 10 by

$$\prod_i \exp\{-a_2[(x_i - x_{\text{site}})^2 + (y_i - y_{\text{site}})^2]\}, \quad (14)$$

in which we used the same parameter for all the solid phases and densities ($a_2 = 0.24 \text{ \AA}^{-2}$) [24, 25]. We have considered four different phases, three commensurate (the $4/7$, widely considered in the standard literature [6–12], the $7/12$ [24, 25], and the newly proposed $1/2$ structure [13]) and an incommensurate triangular one at different densities.

The fact that triangular ^3He solids are incommensurate structures with respect to those of the first hydrogen layer implies that the dimensions of the simulation cells corresponding to those second-layer solids do not have to be (and in fact, they are not) the same as the ones for the hydrogen layer. To avoid mismatch problems between those two sheets, we followed the procedure reported in Refs. [34, 40]. First, we used as the upper simulation cell the larger piece of a triangular solid of a given density that fits in the $48.72 \times 48.22 \text{ \AA}^2$ cell defined by the hydrogen substrate. For instance, if we consider that the upper density for the ^3He triangular solid before the promotion

of ${}^3\text{He}$ to a second Helium layer is the one given in Ref. 12 (0.058 \AA^{-2}) the dimensions of that simulation cell are $44.6 \times 46.34 \text{ \AA}^2$, corresponding to a 10×6 supercell. To take into account all the interactions between any Helium atom and the Hydrogen substrate, we replicate the first layer simulation box to create a nine-cell structure using the vectors that define that Hydrogen sheet. Then, we calculate the corresponding potential terms within a given cutoff distance between the particles in the first and second layer, without using the minimum image convention. That cutoff must be smaller than half the shortest side of the upper simulation cell, in this example 22.3 \AA . On the other hand, the Helium-Helium interactions are calculated in a similar way by using the nine vectors $(0,0), (0, \pm 46.34), (\pm 44.6, 0), (\pm 44.6, \pm 46.34) \text{ \AA}$ to replicate the initial set of second-layer coordinates using the same 22.3 \AA cutoff. The same recipe was employed for the Hydrogen molecules with respect to the second-layer Helium atoms and the molecules closer to the graphite surface. This procedure makes possible to consider any adsorbate density, and not only those which fit exactly the periodicity of the first layer.

In the DMC calculations, $f(\mathbf{R}, t)$ is represented not by an analytical function but by a set of *walkers* [3, 5]. Each walker is defined by a set of coordinates, \mathbf{R} , of all the atoms/molecules of the system. Those positions are evolved in imaginary time by the prescription given in Eqs. 7 and 8 until the local energy of the set of particles, $E_L(\mathbf{R})$, varies stochastically around a stable mean [3, 5]. That would correspond to the limit $t \rightarrow \infty$, limit in which we can calculate other thermodynamic properties. The value of those observables is the average over the set of walkers. We have checked that considering more than 300 walkers leaves the results unchanged. To avoid any influence of the initial configurations on the simulations results, we typically dispose of the first $2 \cdot 10^4$ Monte Carlo steps (a change in all the particles positions in all the 300 walkers) in a typical $1.2 \cdot 10^5$ steps long simulation run. To further avoid spurious influences of a particular DMC history, we averaged the energies of three independent Monte Carlo runs.

Finally, to fully characterize the DMC algorithm, we have to bear in mind that the ${}^3\text{He}$ atoms are fermions. This implies that when we interchange the positions of any two of those particles with the same spin, the total (and its approximation, the trial) function should change sign. We made sure of that by introducing the Slater determinants D^\uparrow and D^\downarrow in Eq. 10. Those determinants impose the nodal structure and the positive and negative regions of the wavefunction. In its simplest form (the one described here and aptly called Fixed-Node diffusion Monte Carlo, FN-DMC), the algorithm does not change the position of those nodes, making the energy derived from it an upper bound to its exact value [3].

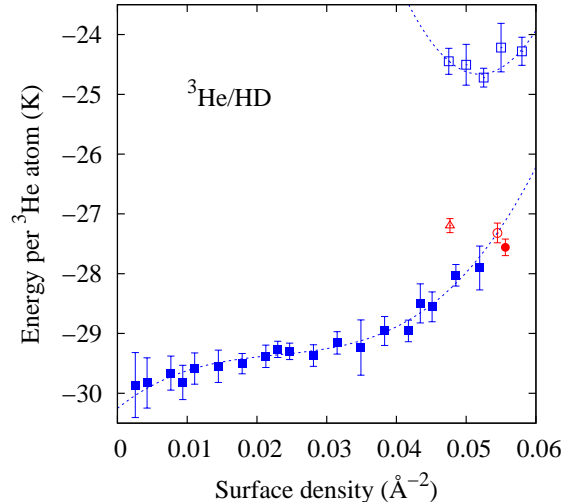


FIG. 1. Energy per ${}^3\text{He}$ atom on a HD layer as a function of the density for a gas structure (solid squares), for an incommensurate triangular solid (open squares), and for different registered phases: $1/2$ (open triangle) $4/7$ (open circle) and $7/12$ (solid circle). The dotted lines correspond to least-squares fittings to cubic polynomials and are intended mainly as guide-to-the-eye. The density range corresponds to the experimental stability region of a single ${}^3\text{He}$ adsorbed on two HD layers [12, 13].

III. RESULTS

The primary output of any DMC calculation is the energy of the ground state of the system under consideration. This implies that we are operating at $T = 0$ and that the energy is equal to the free energy. From that magnitude, we can obtain the phase diagram of ${}^3\text{He}$ adsorbed on top of the different molecular hydrogen substrates. Those results are displayed in Figs. 1-4.

Fig. 1 displays what happens on the HD surface, the one for which we have experimental information [6–13]. The solid squares correspond to the gas phase described by Eq. 10 alone, the dotted line being the result to a least-squares third-order polynomial fit to that set of data. What we observe is that, for that phase, the energy increases monotonically as a function of the ${}^3\text{He}$ density. Moreover, there is no flat region of the curve that we could associate to a liquid-gas transition, as in the first layer of ${}^3\text{He}$ on graphite [38], i.e., at low densities the stable phase is a gas and not a liquid, at least within the accuracy ($\pm 0.3 \text{ K}$) of our calculation. This is similar to what happens to the second-layer of ${}^3\text{He}$ on ${}^3\text{He}$ on graphite [25], but it is at odds with its behavior on ${}^4\text{He}$, where a very dilute liquid phase was predicted [24]. That diluted phase was labeled as liquid because its energy per particle was lower than the corresponding to the infinite dilution limit, i.e., the curve of the energy per Helium atom versus density had a local minimum,

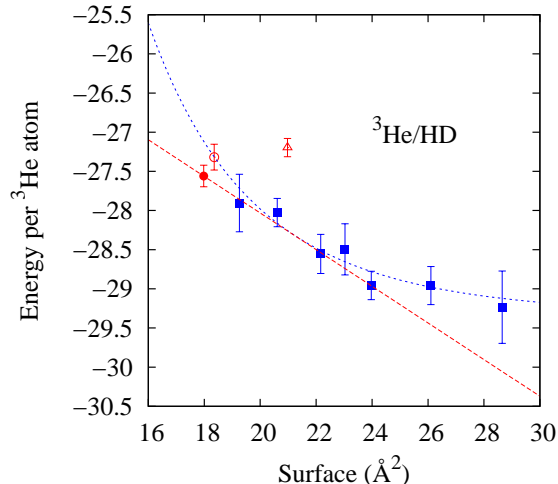


FIG. 2. Energy per ${}^3\text{He}$ atom as a function of the inverse of the density in the range $0.033\text{--}0.060 \text{ \AA}^{-2}$. Symbols have the same meaning as in Fig. 1. Dashed line is the double-tangent Maxwell construction corresponding to the equilibrium between a gas of density $0.048 \pm 0.004 \text{ \AA}^{-2}$ and a $7/12$ commensurate solid.

something not seen here.

The solid structures, described by the product of Eqs. 10 and Eq. 14, differ from each other by the set of crystallographic positions that define them. The energy per Helium atom for a triangular solid is given by the open squares in Fig. 1. This phase is clearly unstable with respect to both the gas and to any of the other registered phases shown in that figure. Those are represented by isolated points: $4/7$ (open circle), $7/12$ (solid circle) and $1/2$ (open triangle). This last structure was proposed to be stable in Ref. 13 and can be built by locating ${}^3\text{He}$ atoms on some of the potential minima produced by three neighboring Hydrogen molecules underneath. In that phase not all such minima are occupied, but only the ones needed to produce a honeycomb lattice on the second layer. Unfortunately, our results do not support the stability of that structure, since its energy per atom is larger than the corresponding to a gas structure of the same density.

The $4/7$ and the $7/12$ structures could be stable, though. To check that, in Fig. 2, we display the double-tangent Maxwell construction (dashed line) between the $7/12$ solid and a gas of density $0.048 \pm 0.004 \text{ \AA}^{-2}$. The slope of that line, that joints the inverse density points with the same derivative of the free energy, corresponds to minus the equilibrium pressure [44]. So, from the two possible Maxwell constructions ($4/7$ -gas, not shown, and $7/12$ -gas), we have to consider only the second, since it corresponds to the lowest pressure value. This line goes from 20.8 \AA^2 (lower surface per particle value for which the gas-like structure is stable, corresponding to a 0.048

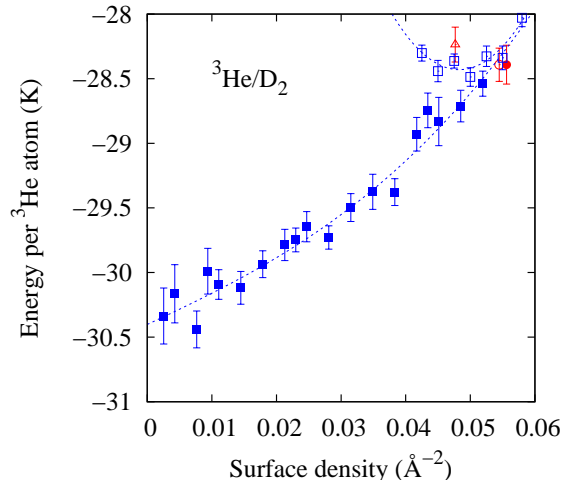


FIG. 3. Same as in Fig. 1 but for ${}^3\text{He}$ on D_2 . The symbols and lines have the same meaning as in that figure.

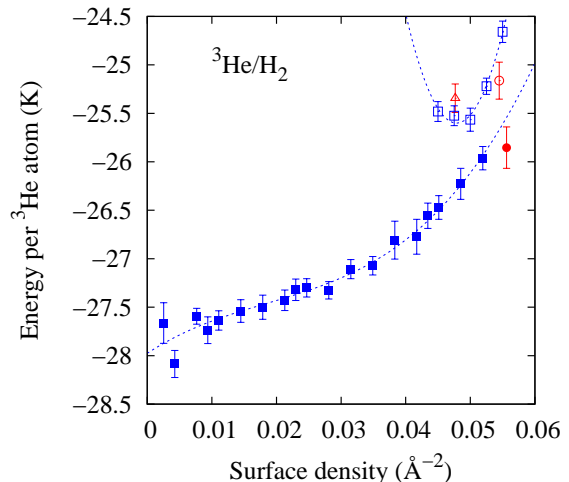


FIG. 4. Same as in previous figures but for ${}^3\text{He}$ on H_2 . The symbols and lines have the same meaning as in Figs. 1 and 3.

 \AA^{-2} helium density) to 18.04 \AA^2 , the inverse of the density of the $7/12$ registered solid. Taking everything into account, we can say that in the $0\text{--}0.048 \text{ \AA}^{-2}$ range, ${}^3\text{He}$ on HD is a gas that, upon further Helium loading changes into a $7/12$ registered solid of density 0.055 \AA^{-2} . This is in overall agreement with the experimental data in the literature [6–13] and similar to what happens on top of ${}^3\text{He}$ [25] and ${}^4\text{He}$ [24].

The DMC algorithm is able to discriminate between ${}^3\text{He}$ adsorbed on similar substrates, as it can be seen in the comparison between Fig. 1 and Figs. 3 and 4. We can

see, for instance, that the Helium binding energies in the respective dilution limits are different from each other: -30.3 ± 0.2 K for HD, -30.4 ± 0.3 K for D₂ and -28.0 ± 0.2 K for H₂, something that depends exclusively on the mass of the molecules of the first layer, all the interaction potentials being equal. This is in agreement to what happens to ³He adsorbed on ⁴He [24] and ³He [25], two substrates with different masses and the same interaction potentials. In the first case, the ³He binding energy in the infinitely dilution limit for a 0.112 \AA^{-2} first layer density was -24.45 ± 0.04 K, to be compared to -22.7 ± 0.1 K for a layer of density 0.109 \AA^{-2} for the lighter isotope. The first value varies very little upon compression of the first layer, increasing to a value of -24.74 ± 0.07 K for an underlying ⁴He density of 0.120 \AA^{-2} . This makes us confident that the ~ 2 K difference between the binding energy of ³He on both helium substrates is due to the mass difference with a very weak dependence on density. All of the above implies that, all things being equal, the larger zero-point motion of a first layer lighter isotope produces a smoother effective potential surface in which the local minima a single atom can sit upon are less deep than for more localized isotopes.

The particular details of the dependences of the energy per ³He atom on the second-layer density for the gas phases are also substrate dependent, but the slopes of those curves as a function of the ³He density are similar (not equal) to each other, as it can be seen in Fig. 5, in which we display all the stable ³He phases for the different hydrogen substrates. In addition, by following the same procedure involving the respective double-tangent Maxwell constructions we have found that the stability range for the gas phases is always $0-0.048 \text{ \AA}^{-2}$, irrespectively of the Hydrogen isotope (see Figs. 6 and 7). Those gases are also in equilibrium with the same 7/12 commensurate phase, all other solid phases being unstable. The details of the adsorption of the unstable triangular solids are also substrate dependent, but are irrelevant for our conclusions since those phases are not experimentally obtained in the range of densities considered here. In any case, the fact that the D₂ substrate produces a phase whose energy per particle is closest to the gas one can be partially ascribed to the fact that a non-moving fixed substrate (or one with smaller zero-point displacements) can artificially boost the stability of a solid phase adsorbed on top, as it can be seen in the case of a second layer of ⁴He on graphite [45].

IV. CONCLUSIONS

By using the DMC method, we were able to calculate the phase diagram of ³He adsorbed on top of a layer of different Hydrogen isotopes. In all cases, those diagrams show stable gases in the $0-0.048 \text{ \AA}^{-2}$ range in equilibrium with 7/12 registered solids. The only difference would come from the Helium-Hydrogen binding energies, something that it can be, but it is hard to be measured

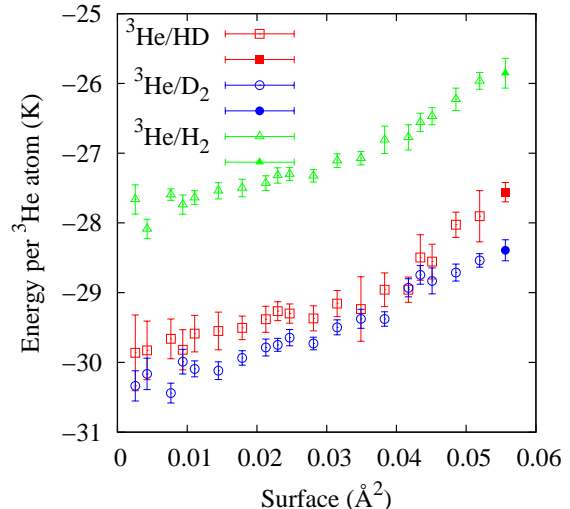


FIG. 5. Energy per ³He atom for the three substrates considered in this work. We display only the stable phases to make comparisons easier. Open symbols, gas phases; solid symbols, 7/12 structures.

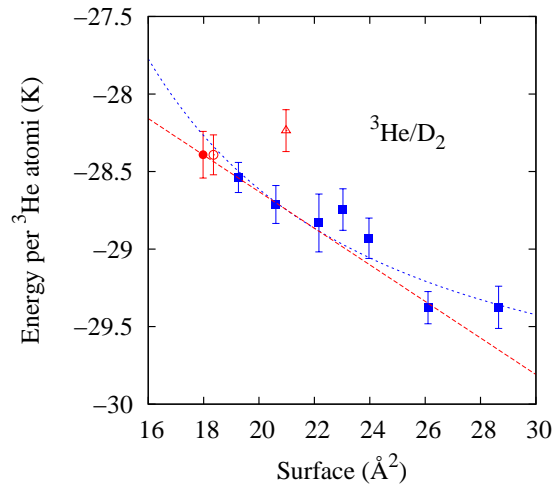


FIG. 6. Same as in Fig. 2 but for ³He on D₂

experimentally. In any case, our results compare reasonably well with experimental data for ³He/HD/HD, that points to the existence of a low-density gas phase that, upon further Helium loading, changes into a commensurate solid. Unfortunately, the nature of that registered phase is different in this work and in the experiment [12]. That difference can be ascribed, at least partially, to the small differences in the densities of the underlying first-layer solid and it is comparable to what happens in a second ³He layer on helium substrates [24, 25]. On the other hand and importantly, we are able to reproduce the

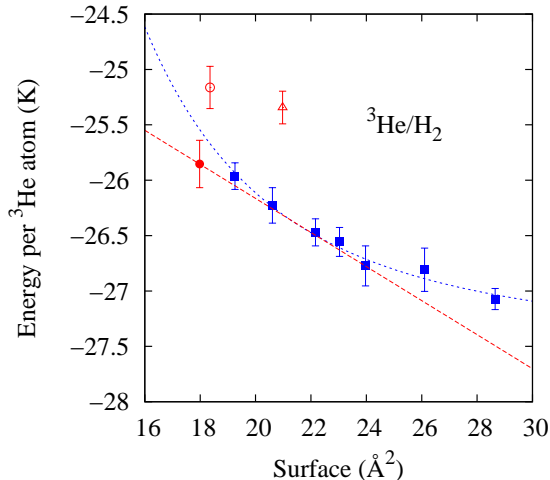


FIG. 7. Same as in Fig. 2 but for ^3He on H_2

fact that the triangular solid is unstable with respect to any other ^3He phase.

ACKNOWLEDGMENTS

We acknowledge financial support from Ministerio de Ciencia e Innovación MCIN/AEI/10.13039/501100011033 (Spain) under Grants No. PID2020-113565GB-C22 and No. PID2020-113565GB-C21, from Junta de Andalucía group PAIDI-205, and AGAUR-Generalitat de Catalunya Grant No. 2021-SGR-01411. We also acknowledge the use of the C3UPO computer facilities at the Universidad Pablo de Olavide. We also thank H. Fukuyama by generously share with us the unpublished work on the $^3\text{He}/\text{HD}/\text{HD}$ system.

-
- [1] N. Metropolis, A.W. Rosenbluth, M.N. Rosenbluth, A.H. Teller, and E. Teller, Equation of state calculations by fast computing machines, *J. Chem. Phys.* **21**, 1087 (1953).
- [2] M. Allen and D. Tildesley, *Computer simulation of liquids, 2nd Ed.* (Oxford university Press, Oxford, 2017).
- [3] B. Hammond, W.A. Lester, and P. Reynolds, *Monte Carlo Methods in Ab Initio Quantum Chemistry* (World Scientific, Singapore, 1994).
- [4] M. H. Kalos, Energy of a boson fluid with lennard-jones potentials, *Phys. Rev. A* **2**, 250 (1970).
- [5] J. Boronat and J. Casulleras, Monte Carlo analysis of an interatomic potential for He, *Phys. Rev. B* **49**, 8920 (1994).
- [6] A. Casey, H. Patel, J. Nyéki, B. P. Cowan, and J. Saunders, Nuclear Magnetism of two dimensional solid ^3He adsorbed on plated graphite, *J. Low Temp. Phys.* **113**, 265 (1998).
- [7] H. Ikegami, R. Masutomi, K. Obara, and H. Ishimoto, Low-temperature magnetization of submonolayer ^3He adsorbed on hd preplated graphite, *Phys. Rev. Lett.* **85**, 5146 (2000).
- [8] H. Ikegami, R. Masutomi, K. Obara, and H. Ishimoto, Low-temperature magnetization of two-dimensional ^3He adsorbed on HD preplated graphite, *Physica B* **284-288**, 222 (2000).
- [9] R. Masutomi, Y. Karaki, and H. Ishimoto, Low temperature magnetization of two dimensional ^3He on itthree layers of HD preplated graphite, *J. Low Temp. Phys.* **126**, 241 (2002).
- [10] A. Casey, H. Patel, M. Siquiera, C. P. Lusher, J. Nyéki, B. P. Cowan, and J. Saunders, Observations of a 'ferromagnetic anomaly' in 2D solid ^3He adsorbed on HD plated graphite, *Physica B* **284-288**, 224 (2000).
- [11] A. Casey, H. Patel, J. Nyéki, B. P. Cowan, and J. Saunders, Evidence for a Mott-Hubbard Transition in a Two-Dimensional ^3He Fluid Monolayer, *Phys. Rev. Lett.* **90**, 115301 (2003).
- [12] M. Kamada, *Quantum phase diagram of monoatomic layer ^3He on graphite* (University of Tokyo, 2017).
- [13] t. b. p. M. Kamada et al., .
- [14] S. W. Van Sciver and O. E. Vilches, Heat-capacity study of the second layer of ^3He adsorbed on Grafoil, *Phys. Rev. B* **18**, 285 (1978).
- [15] D. S. Greywall, Heat capacity of multilayers of ^3He adsorbed on graphite at low millikelvin temperatures, *Phys. Rev. B* **41**, 1842 (1990).
- [16] D. S. Greywall and P. A. Busch, Anomaly in the heat capacity of fluid monolayers of ^3He at low millikelvin temperatures, *Phys. Rev. Lett.* **65**, 64 (1990).
- [17] H. Godfrin, R. E. Rapp, K.-D. Morhard, J. Bossy, and C. Bäuerle, Condensation of ^3He in 21/2 dimensions and indirect exchange in adsorbed films, *Phys. Rev. B* **49**, 12377 (1994).
- [18] K.-D. Morhard, C. Bäuerle, J. Bossy, Y. Bunkov, S. N. Fisher, and H. Godfrin, Two-dimensional Fermi liquid in the highly correlated regime: The second layer of ^3He adsorbed on graphite, *Phys. Rev. B* **53**, 2658 (1996).
- [19] M. Siqueira, J. Nyéki, B. Cowan, and J. Saunders, Heat Capacity Study of the Quantum Antiferromagnetism of a ^3He Monolayer, *Phys. Rev. Lett.* **76**, 1884 (1996).
- [20] E. Collin, S. Triqueneaux, R. Harakaly, M. Roger, C. Bäuerle, Y. M. Bunkov, and H. Godfrin, Quantum Frustration in the "Spin Liquid" Phase of Two-Dimensional ^3He , *Phys. Rev. Lett.* **86**, 2447 (2001).
- [21] D. Sato, K. Naruse, T. Matsui, and H. Fukuyama, Observation of Self-Binding in Monolayer ^3He , *Phys. Rev. Lett.* **109**, 235306 (2012).
- [22] S. Nakamura, K. Matsui, T. Matsui, and H. Fukuyama, Possible quantum liquid crystal phases of helium monolayers, *Phys. Rev. B* **94**, 180501(R) (2016).
- [23] I. Todoshchenko, M. Kamada, J.P. Kaikkonen, Y. Liao, A. Savin, M. Will, E. Sergeicheva, T. S. Abhilash and E. Kauppinen, and P. J. Hakonen, Topologically-imposed

- vacancies and mobile solid ^3He on carbon nanotube, Nat. Commun. **13**, 5873 (2022).
- [24] M. C. Gordillo and J. Boronat, ^3He on preplated graphite, Phys. Rev. B **94**, 165421 (2016).
- [25] M. C. Gordillo and J. Boronat, Fluid and registered phases in the second layer of ^3He on graphite, Phys. Rev. B **97**, 201410 (2018).
- [26] M. C. Gordillo, H_2 on corrugated graphene: Diffusion Monte Carlo calculations, Phys. Rev. B **88**, 041406 (2013).
- [27] Q. Wang and J. Johnson, Hydrogen adsorption on graphite and in carbon slit pores from path integral simulations, Mol. Phys. **95**, 299 (1998).
- [28] W. E. Carlos and M. W. Cole, Interaction between a He atom and a graphite surface, Surf. Sci. **91**, 339 (1980).
- [29] G. Stan and M. W. Cole, Hydrogen adsorption in nanotubes, J. Low Temp. Phys. **110**, 539 (1998).
- [30] R. Aziz, F.R.W. McCourt, and C. K. Wong, A new determination of the ground state interatomic potential for He_2 , Mol. Phys. **61**, 1487 (1987).
- [31] I. F. Silvera and V. V. Goldman, The isotropic intermolecular potential for H_2 and D_2 in the solid and gas phases, J. Chem. Phys. **69**, 4209 (1978).
- [32] R. Barnett and K. Whaley, Monte Carlo study of impurities in quantum clusters: H_2 , $^4\text{He}_N$, $N=2-19$, J. Chem. Phys. **96**, 2953 (1992).
- [33] M. C. Gordillo, $^4\text{He}/\text{H}_2$ binary clusters: A path-integral Monte Carlo study, Phys. Rev. B **60**, 6790 (1999).
- [34] M. C. Gordillo and J. Boronat, Supersolidity in the second layer of para- H_2 adsorbed on graphite, Phys. Rev. B **105**, 094501 (2022).
- [35] K. E. Schmidt, M. A. Lee, M. H. Kalos, and G. V. Chester, Structure of the ground state of a fermion fluid, Phys. Rev. Lett. **47**, 807 (1981).
- [36] J. Boronat, in *Microscopic Approaches to Quantum Liquids in Confined Geometries*, edited by E. Krotscheck and J. Navarro (World Scientific, Singapore, 2002).
- [37] J. Casulleras and J. Boronat, Progress in Monte Carlo Calculations of Fermi Systems: Normal Liquid ^3He , Phys. Rev. Lett. **84**, 3121 (2000).
- [38] M. C. Gordillo and J. Boronat, Liquid and solid phases of ^3He on graphite, Phys. Rev. Lett. **116**, 145301 (2016).
- [39] H. F. H. Wiechert and H. Lauter, Heat-capacity and neutron-diffraction studies of HD monolayers physisorbed on graphite, Surf. Sci. **269/270**, i452 (1992).
- [40] M. C. Gordillo and J. Boronat, Second layer of H_2 and D_2 adsorbed on graphene, Phys. Rev. B **87**, 165403 (2013).
- [41] H. Wiechert, in *Excitations in Two-Dimensional and Three-Dimensional Quantum Fluid*, edited by A. Wyatt and H. Lauter (Plenum, New York, 1991).
- [42] M. C. Gordillo and J. Boronat, Phase diagram of H_2 adsorbed on graphene, Phys. Rev. B **81**, 155435 (2010).
- [43] C. Carbonell-Coronado and M. C. Gordillo, Phase diagram of D_2 adsorbed on graphene and graphite, Phys. Rev. B **85**, 155427 (2012).
- [44] D. Chandler, *Introduction of modern statistical mechanics* (Oxford university Press, New York, 1987).
- [45] P. Corboz, M. Boninsegni, L. Pollet, and M. Troyer, Phase diagram of ^4He adsorbed on graphite, Phys. Rev. B **78**, 245414 (2008).